Geothermics 110 (2023) 102677

Contents lists available at ScienceDirect

Geothermics

journal homepage: www.elsevier.com/locate/geothermics

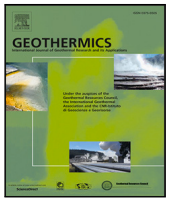

Thermoelectric generator for high temperature geothermal anomalies: Experimental development and field operation

Patricia Alegría, Leyre Catalán *, Miguel Araiz, Álvaro Casi, David Astrain

Institute of Smart Cities, Public University of Navarre, Pamplona, Spain

ARTICLE INFO

Keywords:
Geothermal energy
Thermoelectric generator
Heat exchanger
Thermoelectricity
Phase change

ABSTRACT

In the current climate and energy context, it is important to develop technologies that permit increase the use of renewable sources such as geothermal energy. Enhancing the use of this renewable source is particularly important in some places, due to its availability and the enormous dependence on fossil fuels, as is the case of the Canary Islands. This work proposes the use of thermoelectric generators with heat exchangers working by phase change to transform the heat from the shallow high temperature geothermal anomalies on the island of Lanzarote directly into electricity, since the use of conventional geothermal power plants would not be possible because they would damage the protected environment. To bring this proposal to reality, this work has succeeded in developing and field-installing a geothermal thermoelectric generator that operates without moving parts thanks to its phase-change heat exchangers. This robust generator do not require maintenance nor auxiliary consumption, and produces a minimal environmental impact, it is noiseless, and the use of water as working fluid makes it completely harmless.

The developed device consists of a thermosyphon as hot side heat exchanger, thermoelectric modules and cold side heat exchangers also based in phase change. Tests were carried out in the laboratory at various heat source temperatures and varying the number of thermoelectric modules. It was determined that installing more modules decreases the efficiency per module (from 4.83% with 4 modules to 4.59% with 8 modules at a temperature difference between sources of 235 °C), but for the number of modules tested the total power increases, so the field installation was carried out with 8 modules. After the good results in the laboratory, it was satisfactorily installed at Timanfaya National Park (Lanzarote, Spain) in a borehole with gases at 465 °C. This generator presents a maximum output power of 36 W (4.5 W per module), and is generating 286.94 kWh per year, demonstrating the great potential of the developed thermoelectric generators to build a larger-scale renewable installation.

1. Introduction

The transition to the use of renewable energy sources is a global necessity and a challenge. Many countries are making efforts to promote renewable energies in order to reduce greenhouse gas emissions and mitigate global warming so as not to exceed the 1.5 °C of temperature increase since preindustrial levels established in the Paris Agreement (United Nations, 2016). The European Commission, through the European Green Pact, adopted in 2019 a set of proposals to reduce net greenhouse gas emissions by at least 55% by 2030 and 100% by 2050 compared to 1990 levels (European Comission, 2020). Although there has been a large increase in energy produced from renewable sources in recent decades, even today only 12.6% of the world's primary energy is renewable (REN21, 2021). As a consequence, the need for further technological development and the installation of more renewable systems becomes evident.

There exist renewable sources that have not achieved enough development, such as geothermal energy, which contributed less than 3% to the worldwide electricity production in 2021 (REN21, 2021). However, geothermal energy has a great potential and the advantage that it is not an intermittent source, but is always available, regardless of the weather.

The need for new technologies to promote the use of this renewable source is higher in some regions like the Canary Islands (Spain), which have a great geothermal potential that is currently untapped. These islands, with a 98% dependence on fossil fuels for their primary energy (Red Eléctrica de España, 2021) and with an isolated electrical system, require a deeper development of technologies that enhance their decarbonization. Thus, the Sustainable Energy Strategy in the Canary Islands, which is part of the Recovery, Transformation and

* Corresponding author.
E-mail address: leyre.catalan@unavarra.es (L. Catalán).

https://doi.org/10.1016/j.geothermics.2023.102677
Received 21 November 2022; Received in revised form 20 January 2023; Accepted 5 February 2023
Available online 9 February 2023

Nomenclature

Variables

ΔT	Temperature difference (°C)
$\dot{Q}$	Heat flux (W)
η	Efficiency
h	Heat transfer convection coefficient (W/m^2 K)
k	Thermal conductivity (W/m K)
m	Number of thermoelectric modules in a GTEG
P	Electric power (W)
R	Thermal resistance (K/W)
T	Temperature (°C)
v	Velocity (m/s)

Subscripts and Superscripts

amb	Ambient
b	Boiling
C	Cold side of the thermoelectric module
c	Condenser/Condensation
$cond$	Conductive
$const$	Constriction
$conv$	Convective
$crit$	Critical temperature
e	External
eq	Equivalent
H	Hot side of the thermoelectric module
i	Internal
l	Liquid
v	Vapour

Abbreviations

CHE	Cold side Heat Exchanger
EGS	Enhanced Geothermal System
EU	European Union
GTEG	Geothermal Thermoelectric Generator
HDR	Hot Dry Rock Field
HHE	Hot side Heat Exchanger
S	Source of heat (In laboratory: TPCT wall. In field: Hot gasses.)
TEG	Thermoelectric Generator
TEM	Thermoelectric Module
TNP	Timanfaya National Park
TPCT	Two Phase Closed Thermosyphon

Resilience Plan, financed by *EU Next Generation* funds, includes programme number 6, whose objective is to promote innovative projects in the field of energy, with innovative technologies that permit the use of high temperature geothermal energy. In fact, one of the lines of action focuses on medium/high temperature geothermal energy by promoting research to demonstrate the viability of the geothermal resource on the islands for use in electricity generation (Government of the Canary Islands et al., 2022).

The Timanfaya National Park (TNP), in Lanzarote (Canary Islands, Spain), is one of the most important shallow hot dry rock fields in the world. The geothermal anomalies are caused by the presence of a lava body at a depth of 1 km, corresponding to the last eruptions of 1730 and 1824 (Garcia et al., 2009). Thus, geothermal gases in this zone are 98% nitrogen due to the fact that the air that hits the porous surface of some volcanic cones is heated by the magma and rises by density difference to the surface (Troll and Carracedo, 2016; Arana et al., 1973). However, the conventional technology to exploit this type of fields requires the drilling of several wells, in which water is inserted at high pressures to fracture the rock and create an artificial reservoir. This method, called EGS (Enhanced Geothermal Systems), is economically very costly and susceptible to collateral problems such as induced seismicity, high visual impact and high water and maintenance costs (Ganguly and Kumar, 2012; Li et al., 2015). Thermoelectric generators, despite their low efficiency compared to conventional geothermal plants (Breede et al., 2013), would avoid all these drawbacks, favouring geothermal generation in a more cost-effective, scalable and environmentally friendly way. These geothermal thermoelectric generators (GTEGs) could be implemented in any shallow geothermal anomaly in the world, but in the Canary Islands this thermoelectric technology is especially important (Ministerio para la Transición Ecológica y el Reto Demográfico, 2020). Furthermore, GTEGs have been identified as the only feasible solution to transform geothermal energy in the island of Lanzarote into electricity (Government of the Canary Islands, 2019, 2021).

A geothermal thermoelectric generator is a device that directly transforms geothermal energy into electricity thanks to its main component, the thermoelectric module (TEM). Thermoelectric modules are solid-state devices that, thanks to the *Seebeck* effect, are capable of transforming a heat flux produced by a temperature difference between its sides into an electric current. Its efficiency is higher with a higher thermal difference. Hence, heat exchangers are very important, as they are responsible of the temperatures achieved in the TEM's sides. They must transport the heat from a geothermal source to the hot face of the TEM, and from the cold face of the TEM to the heat sink, which is usually the ambient.

Due to their low efficiency, the use of thermoelectric generators has been sidelined to militar or aerospace applications, where their advantages such as robustness are more important than their efficiency. The development of thermoelectric generators for civil applications is meagre, and few experimental studies of GTEGs are found in the literature. Some of these studies focus on applications that require low power supply, such as IoT devices. One example is a thermoelectric generator that Mona et al. (2022) tested in a hot spring in Thailand, obtaining a power output of 0.4 mW. Dell et al. (2018) developed a thermoelectric generator that was able to produce more than 5 W (0.83 W per TEM) in with a 130 °C difference between the ambient temperature and the surface of a geothermal steam pipe in Iceland. Ahiska and Mamur (2013) designed and tested a portable thermoelectric generator, also for low geothermal temperatures, obtaining a maximum power output of 41.6 W (2.08 W per TEM) when the temperature difference between the module surfaces was 67 °C. Zhao et al. (2022) developed a geothermal thermoelectric generator with a passive heat pipe heat exchanger on the hot side, but water-cooled with a pumping system on the cold side, achieving a maximum power output of 10.85 W in the laboratory with 4 modules, but without taking into account the auxiliary consumption of the pumping system for cooling the cold side of the TEMs. In a higher scale, Suter et al. (2012) modelled and optimized a 1 kWe thermoelectric stack for geothermal heat conversion with hot water inlet and outlet temperatures of 140 °C and 20 °C. All these are laboratory or computer studies and all of them include moving parts to circulate a fluid, which entails auxiliary consumptions. For instance, Li et al. (2021) developed and tested a GTEG at the *Bottle Rock* Geothermal Power Plant (California, USA), using steam from a geothermal well as a heat source, and cooled by a water flow on the cold side. They estimated that this device can generate 500 W (3.6 W per TEM), but again, it requires moving parts to recirculate the cooling fluid and a deep geothermal installation. The use of heat exchangers with fluid circulation requires the use of moving parts, which entails a need for maintenance and auxiliary consumptions, losing the main advantage of thermoelectric

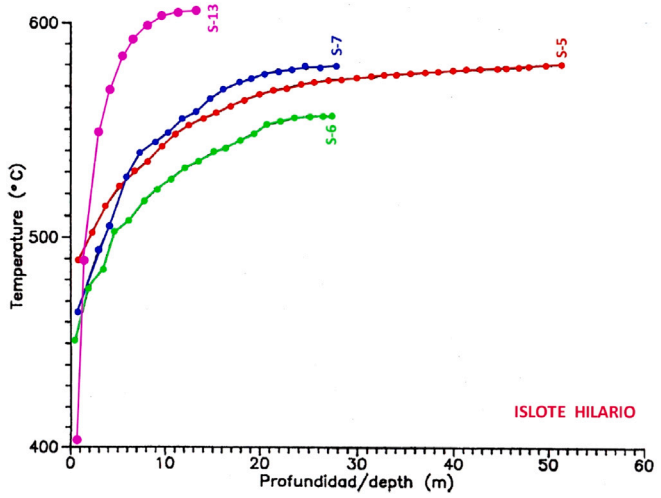

Fig. 1. Temperature profile of the boreholes in *Islote Hilario* (Instituto Geológico Minero Español, 1992).

modules, their robustness. The only GTEG developed without moving parts are the ones developed by Catalan et al. (2020b,c). They firstly developed a geothermal thermoelectric generator that uses volcanic heat to supply electricity to volcanic monitoring stations, making them totally autonomous, with results of 0.49 W generated by TEM. This innovative autonomous monitoring system is operating in the fumaroles of Teide volcano since 2019.

To go further, based on the conditions of the Timanfaya National Park, Catalan et al. (2019) built and tested in the laboratory a prototype consisting of a two-phase closed thermosyphon (TPCT) as a heat exchanger on the hot side, two thermoelectric modules, and considered different heat exchangers on the cold side: fan-assisted finned dissipators and loop thermosyphons, both with different geometries. They demonstrated that thermosyphons were the best alternative due to their low thermal resistance and, above all, their lack of moving parts nor auxiliary consumption, which led to a maximum net power generation of 3.9 W per module with a temperature difference of 180 °C (200 °C on the hot side and 20 °C as ambient temperature), 54% more than with finned dissipators. Hence, they patented an unprecedented GTEG, whose heat exchangers' principle of operation was phase change. They also developed a computational model based on the finite difference method, capable of predicting the behaviour of this type of devices. Following their study, Alegria et al. (2022) developed a new GTEG in laboratory without moving parts achieving a generation of 36 W with 16 TEMs and a temperature difference between sources of 160 °C. But there are areas in the TNP where high temperature geothermal anomalies can be found, with boreholes that present gases rising at temperatures of 500 °C, as can be seen in Fig. 1.

Taking as a base the knowledge acquired in the previous studies of GTEGs, this work goes a step further, developing a new device without moving parts, with the advantages this entails, adapted to the highest temperatures found in the volcanic area of Lanzarote and reaching the new milestone of installing and testing in field. This innovative kind of geothermal thermoelectric generator based on phase change is field-tested during more than one year without maintenance, to leverage these currently squandered high temperatures and to demonstrate the feasibility of a high-scale installation to make the facilities at TNP self-sufficient and renewable powered.

Thus, Section 2 describes the computational design of the generator. Then, Section 3 contains the laboratory development of the parts of the geothermal thermoelectric generator, including the whole assembly. Afterwards, in Section 4, the installation in Timanfaya National Park is carried out and the results of its field operation are shown. And finally, Section 5 exposes the conclusions of this work and the future lines.

2. Computational design

The developed hot side heat exchanger (HHE) is based on the working principle of phase change due to the mentioned advantages, but for a detailed design, it was necessary to simulate its behaviour with a computational model. The model employed is the one developed by Catalan et al. (2020a) which, for the first time, considers heat exchangers based on phase change at both sides of the TEMs. This model is based on the thermal–electrical analogy derived from the application of the implicit finite difference method to heat conduction equation. Its basic idea consists in discretizing the system in a finite number of nodes and obtaining the solution of the problem for those nodes. For the implementation of this computational model, the environment *MATLAB* has been employed and each part of the GTEG has been modelled by means of its corresponding thermal resistance.

The hot side heat exchanger has a total thermal resistance R^H_{total} that corresponds to Eq. (8). It is a two phase closed thermosyphon (TPCT) absorbing heat by convection from the hot gases of the borehole, so this total resistance of the hot side is the sum of the convection thermal resistance (R^H_{conv}, Eq. (1)), the conduction in the evaporation zone (R^H_{k1}, Eq. (2)), the boiling and condensation resistances (R^H_b and R^H_c), whose coefficients are calculated according to Forster and Zuber (1955) and Rohsenow et al. (1998), respectively, and finally, the last thermal resistance in the condensation zone (R^H_{k2}, Eq. (7)), which is composed of a conduction resistance ($R^H_{k2,cond}$, Eq. (5)) and a constriction resistance ($R^H_{k2,const}$, Eq. (6)) due to the fact that condensation occurs in an area bigger than that of the module.

$$R^H_{conv} = \frac{1}{h^H_{conv} \cdot A^H_{conv} \cdot \eta^H_{fin}} \tag{1}$$

$$R^H_{k1} = \frac{\ln\left(D^H_e / D^H_i\right)}{2 \cdot \pi \cdot L \cdot k} \tag{2}$$

$$R^H_b = \frac{1}{h^H_b \cdot A^H_b} \tag{3}$$

$$R^H_c = \frac{1}{h^H_c \cdot A^H_c} \tag{4}$$

$$R^H_{k2,cond} = \frac{e^H_c}{k^H \cdot A^H_c} \tag{5}$$

$$R^H_{k2,const} = \frac{\Psi^H}{N_{TEM} \cdot k^H \cdot \sqrt{A_{TEM}}} \tag{6}$$

$$R^H_{k2} = R^H_{k2,cond} + R^H_{k2,const} \tag{7}$$

$$R^H_{total} = R^H_{conv} + R^H_{k1} + R^H_b + R^H_c + R^H_{k2} \tag{8}$$

Then, the thermoelectric modules' thermal resistance (R^{TEM}_{total}) is composed by that of the n-type semiconductors ($R_{n(i,i+1)}$), the p-type semiconductors ($R_{p(i,i+1)}$), the unions (R^H_u and R^C_u) and the insulation (R^H_{ins} and R^C_{ins}).

$$R_{n(i,i+1)} = \frac{L_n/9}{N_{TEM} \cdot N_{tc} \cdot k_{n(i,i+1)} \cdot A_n} \quad i = 1-9 \tag{9}$$

$$R_{p(i,i+1)} = \frac{L_p/9}{N_{TEM} \cdot N_{tc} \cdot k_{p(i,i+1)} \cdot A_p} \quad i = 1-9 \tag{10}$$

$$R^H_u = R^C_u = \frac{L_u}{N_{TEM} \cdot N_{tc} \cdot k_u \cdot A_u/2} \tag{11}$$

$$R^H_{ins} = R^C_{ins} = \frac{L_{ins}}{N_{TEM} \cdot k_{ins} \cdot A_{ins}} \tag{12}$$

$$R^{TEM}_{total} = R_{n(i,i+1)} + R_{p(i,i+1)} + R^H_u + R^C_u + R^H_{ins} + R^C_{ins} \tag{13}$$

And in this computational study, the thermal resistance of the cold side heat exchangers (CHE), which also work by phase change, has been introduced as a constant thermal resistance ($R^C = 0.33\,\mathrm{K/W}$) obtained

Table 1
Results of the computational simulation.

Number of TEMs	h_S (W/m^2 K)	T_l (°C)	T_H (°C)
8	10	187.10	154.07
	20	266.72	217.46
4	10	253.96	227.99
	20	333.98	298.93

by the experimental characterization of the CHE in the laboratory, explained in Section 3.

The thermal–electrical analogy is actually derived from the application of the implicit finite difference method to heat conduction equation, so with all the thermal resistances, the numerical resolution is carried out in each node i by an iterative method with Eq. (14), considering a permanent regime and being j each adjacent node.

$$\sum_j \frac{T_j - T_i}{R_{ij}} + \dot{Q}_i = 0 \tag{14}$$

The main objective of this computational simulation is to find a suitable design. Thus, details such as the working fluid, the thickness of the wall of the TPCT, the volume of water that fills it, the type of thermoelectric modules depending on the temperatures they need to resist, and the number of TEMs to install have to be determined. The following are the boundary conditions in this calculation; the temperature of the hot source or borehole (T_S) was considered to be 500 °C (Instituto Geológico Minero Español, 1992), the cold source or ambient temperature (T_{amb}) was considered to be 25 °C, the material was stainless steel and water as the working fluid. The entrance parameters to the model are the following:

- Borehole gas temperature (°C)
- Flow rate of gases leaving the borehole (m^3/h)
- Borehole diameter (m)
- Number of thermosyphons per borehole
- Thermosyphon diameter (m)
- Thermosyphon length (m)
- Height of fluid inside the thermosyphon (m)
- Wall thickness of the thermosyphon (m) and material
- Number of fins in the thermosyphon
- Length of fins in the thermosyphon (m)
- Thickness of fins in the thermosyphon (m)
- Number of thermoelectric modules
- Number of levels with 2 thermoelectric modules in series
- Ambient temperature (°C)
- Wind speed (km/h)

Thanks to the model, the temperature in the wall of the boiling part of the TPCT and the temperature of the hot side of the modules were determined and are shown in Table 1, varying the convection coefficient of the hot gases (h_S) between 10 and 20 W/m^2 K, because the velocity of these gases was unknown. The number of TEMs installed was also varied from 4 to 8. The reason is that the installation will be carried out in a protected national park, and to minimize the visual impact, the maximum height requirement is 0.5 m from the ground. To meet these height restrictions, due to the configuration of the cold side heat exchangers, which is explained in Section 3, the developed 3D designs indicated that a maximum number of 8 TEMs could be installed distributed in 4 levels of pairs of modules, each one with its corresponding CHE, as shows Fig. 2. The minimum was estimated at 2 levels (4 TEMs) so as not to overpass the maximum operation temperature of the TEMs, taking into account the computational study.

One of the requirements to be met by the thermoelectric generator developed is the minimum possible environmental impact. For this reason, the use of water as working fluid is preferred, as well as for its price and its safety for people and for the environment, despite its critical temperature (T_{crit}) of 374 °C (Lemmon et al., 2018), from which phase change would cease to occur and the TPCT would lose its working principle. Then, the corresponding pressure of the water inside the thermosyphon must be calculated in order to determine the thickness of the TPCT, as well as the quality of the vapour, the fluid height and the vaporization enthalpy to make sure that there is always a biphasic mixture inside the TPCT and phase change works.

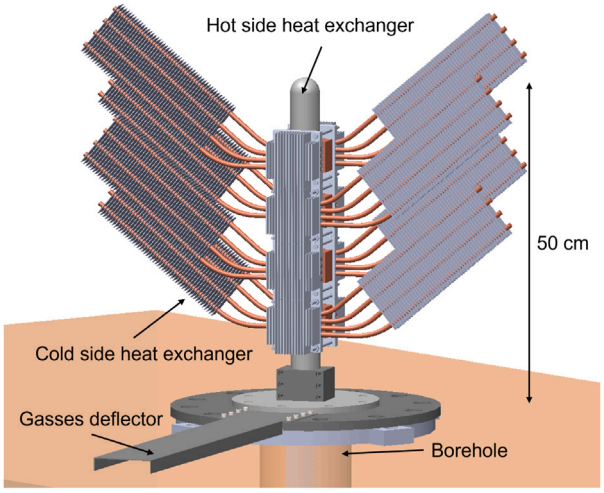

Fig. 2. Design of the GTEG.

Table 2
Calculation of the pressure ($P_l l$), liquid mass (m_l), vapour mass (m_v), quality of vapour (x), liquid height (L_l) and vaporization enthalpy (h_{l-v}) in the TPCT at different temperatures of the water (T_l).

T_l (°C)	P_l (bar)	m_l (kg)	m_v (kg)	x	L_l (m)	h_{l-v} (kJ/kg)
175	8.93	0.4921	0.0079	0.016	0.486	2031.70
200	15.55	0.4866	0.0134	0.027	0.496	1939.70
225	25.50	0.4784	0.0216	0.043	0.506	1835.40
250	39.76	0.4664	0.0336	0.067	0.515	1715.20
275	59.46	0.4488	0.0512	0.102	0.521	1574.30
300	85.88	0.4227	0.0773	0.155	0.523	1404.60
325	120.51	0.3811	0.1189	0.238	0.514	1190.80
350	165.29	0.3020	0.1980	0.396	0.463	892.75

On the one hand, the simulation determined that the working temperature range on the outer wall of the thermosyphon (T_l) varies between 187.10 °C and 333.98 °C, depending on the convection coefficient with the air inside the borehole and the number of thermoelectric modules installed. Thus, the rest of the calculations were made at a temperature range from 175 °C to 350 °C. Table 2 shows the results for the required values.

To determine the pressure corresponding to the water inside the thermosyphon (P_l), an infinitesimal TPCT thickness was considered, so that the inside and outside temperature of the pipe are equal and the water pressure is more restrictive. At a temperature of 350 °C, the water pressure is 165.29 bar (Lemmon et al., 2018), so a 5 mm thick AISI 316L stainless steel tube was selected for the manufacture of the thermosyphon, which is not only capable of withstanding this pressure, but has other advantages such as that the working pressure does not decrease as drastically with temperature like other types of stainless steel as AISI 304 (Sandvik, 2022). Although the thermal conductivity of copper is much higher, 385 W/m K, compared to the 14 W/m K of 316L steel at room temperature, this material has better mechanical properties which make it more suitable for working at high temperatures. The outer diameter of this tube was 48 mm (38 mm inner diameter), dimensions based on the computational study carried out by Catalan et al. (2020a).

Considering the density of water at different temperatures and applying the equation system below, as well as Eqs. (15) and (16), the quality of vapour (x) and the liquid height (L_l) were calculated. The vaporization enthalpy was obtained from Lemmon et al. (2018).

$$\begin{cases} m_{tot} = m_l + m_v \\ v_{tot} = v_l + v_v \end{cases}$$

$$x = \frac{m_v}{m_l + m_v} \tag{15}$$

$$L_l = \frac{v_l}{\frac{\pi}{4} \cdot D_{int}^2} \tag{16}$$

As can be seen in Table 2, even in the most critical temperature case, there would still be vapour–liquid mixture inside the thermosyphon and, therefore, phase change would still occur. The liquid water would reach a height inside the thermosyphon of 0.486 m at 175 °C and of 0.463 m at 350 °C. Since it should never operate at such a high temperature, there will be no peril of all the water inside the thermosyphon being vaporized and no phase change occurring.

Taking into account the simulation, the TPCT will consist of a 2 m stainless steel tube of AISI 316L, with an outer diameter of 48 mm, filled with 0.43 l of water. It has also two caps and a valve in the upper cap in order to purge the air that could remain inside the TPCT worsing its behaviour.

The water inside will absorb the heat rising through the borehole and will transmit it to the upper part where the heat will be transferred to the hot side of the thermoelectric modules. The rest of the heat that is not transformed into electricity will be dissipated into the environment by the cold side heat exchangers, whose configuration is based on the previous research of Alegria et al. (2022). Given that Catalán et al. demonstrated that the best heat exchangers for the application considered here are those whose operation principle is phase change (Catalan et al., 2019), the CHEs consist of four heat pipes of 450 mm length and 8 mm diameter press-fitted into a 80 mm × 90 mm heat sink with 17 aluminium fins of 14 mm × 1.5 mm, whose 14.5 mm flat base was perfectly adapted to the planar surface of the TEM. Between the base of the heatsink and the module, a graphite foil was added, which improves the contact between the two parts, thus reducing the contact resistance. Aluminium fins were inserted into the heat pipes every 5 mm to increase the heat exchange area, improving the convection with the wind and the heat dissipation (Casi et al., 2020). The research developed by Alegría shown that the CHEs were more compact by placing the heat pipes horizontally and bending them 40°, as they could be installed in a row, so the CHE employed in this work, which is shown in Fig. 3, has the same bending angle (Alegria et al., 2022).

3. Laboratory tests and development

The function of a cold side heat exchanger (CHE) is to transport the heat as efficiently as possible from the cold side of the thermoelectric modules to the ambient in order to make its temperature as close as possible to that of ambient, thus achieving the highest possible ΔT in the TEM. Then, prior to the assembly of the complete generator, a thermal characterization of these heat exchangers was carried out to obtain the value of their thermal resistance and to ensure that their operation was adequate. The characterization assembly was made using the elements shown in Fig. 3, so that different known heat flows ($\dot{Q}$) passed through the exchanger by means of a heating plate. Following Eq. (17), the thermal resistance of the heat exchanger, R_{CHE}, was calculated by measuring the temperature difference between the internal surface of the heat exchanger, T_C, and the environment, T_{amb}.

$$R_{CHE} = \frac{T_C - T_{amb}}{\dot{Q}} \tag{17}$$

These tests were carried out inside a climatic chamber in order to maintain a constant ambient temperature equal to 20 °C, with an air velocity of 1 m/s. The obtained results are shown in Fig. 4, which shows that there is not a significant variation in thermal resistance as the heat flux increases, with an average value of 0.33 K/W. The variations, less than 8%, may be due to the measurement uncertainties, which were calculated according to the method shown in Coleman and Steele (2018), using the instruments whose reliability is shown in Table 3. This way, each thermal resistance has associated a variation called expanded uncertainty, so that the value of each thermal resistance includes the uncertainty value, which depends on the random and systematic errors.

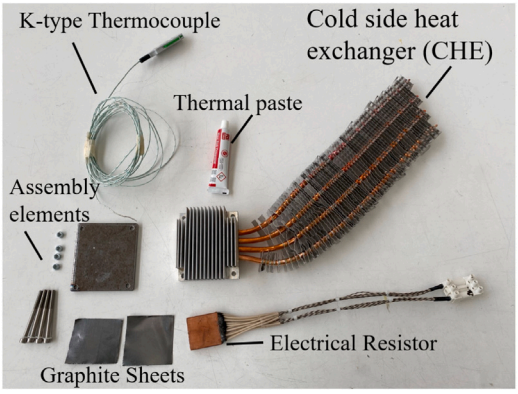

Fig. 3. Elements employed to carry out the CHE characterization tests.

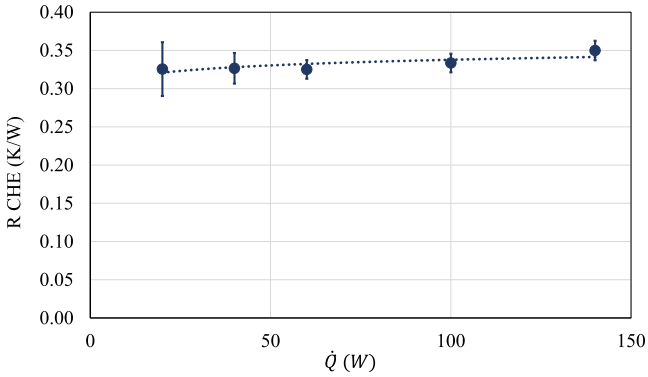

Fig. 4. Thermal characterization of the CHE.

After determining the hot and the cold heat exchangers comes the complete assembly of the GTEG. The main part are the thermoelectric modules, which are responsible for transforming a heat flow directly into electricity. The commercial modules that are most widely used industrially due to their operating temperature range, availability and affordability are Bismuth-Telluride (Bi_2Te_3) (Champier, 2017; Saberi and Sajjadi, 2022) modules. Thus, the ones used in this research work are the *TG12-8LS* model from the manufacturer *Marlow*, which are composed of 127 Bismuth-Telluride thermocouples and are capable of operating at temperatures up to 230 °C.

Although the air outlet temperature in the borehole is around 500 °C, according to the previous computational study, it is expected that the TEMs will not reach this temperature due to the thermal drop from the borehole gases to the hot face of the modules. The hot side working temperatures are expected to be lower than the maximum operation temperature of the modules, except in the worst case (high convection coefficient and only 4 thermoelectric modules).

A very important design factor is the number of thermoelectric modules to be installed in the generator. As explained Catalán and Alegría, both the low thermal resistances of the exchangers and a number of modules close to the optimum is very important for the power that a

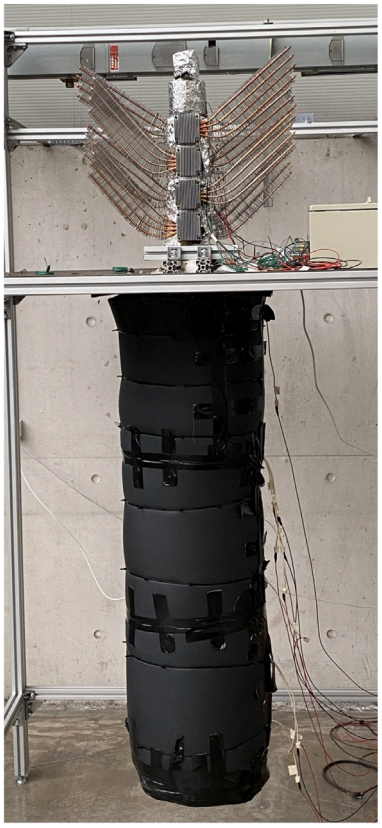

Fig. 5. Geothermal thermoelectric generator (GTEG) installed in the laboratory.

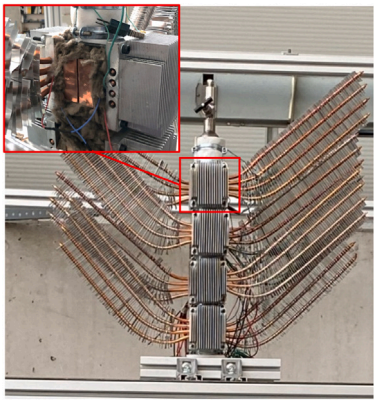

Fig. 6. Upper part of the GTEG.

GTEG is able to generate, as it is already known that the total generated power depends on the number of thermoelectric modules, presenting an optimum, from which the total power decreases (Catalan et al., 2020a; Alegria et al., 2022). This phenomenon occurs because these generators have one CHE per module installed, and all the modules share the same HHE. Thus, experimental tests were be carried out in the laboratory to determine the optimum number of modules to be installed.

To simulate the hot temperatures of the geothermal borehole, rope heaters were installed along the 1.5 m of TPCT that would be inserted in the ground and this part was insulated with a 80 cm diameter of rock wool and a 2 cm layer of neoprene. The complete GTEG installed in the laboratory can be seen in Fig. 5 and with more detail in Fig. 6.

For both laboratory and field tests, temperature probes and devices were installed to measure the power generated by the modules throughout the prototype. The position of the sensors can be seen in Fig. 7 and

Table 3
Resolution and accuracy of the measuring instruments.

Instrument	Measure	Accuracy	Resolution
INA219 sensor	Voltage (V)	±0.02	0.01
INA219 sensor	Current (A)	±0.02	0.01
K-type thermocouple	Temperature (°C)	±0.5	0.1
Anemometer Ahlborn FVAD15-H	Air velocity (m/s)	±1.5%	0.01

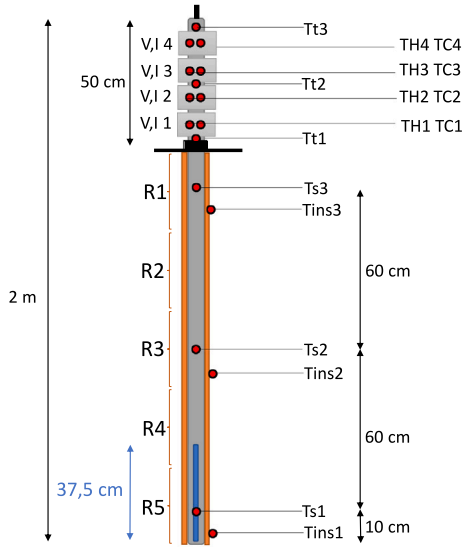

Fig. 7. Schematics of the rope heaters, temperature, voltage and intensity sensors installed in the laboratory.

their characteristics, as well as the table of instrument resolutions and accuracies, are detailed in Table 3.

Laboratory tests were carried out under forced convection conditions using a fan that produced a wind of 1.5 m/s, simulating the wind conditions that occur naturally in the Timanfaya National Park, so the consumption of this fan will not be taken into account in the total power generated by the thermoelectric device.

Tests were carried out with different temperatures of the hot source, varying in the temperature range expected to be obtained in the lower external part of the thermosyphon once installed in the corresponding borehole in Timanfaya (220 °C, 258 °C and 290 °C). As mentioned, the objective is to determine the total power that it is capable of generating at different temperatures, as well as the power per module and to determine if installing more levels of thermoelectric modules in the device will harm or improve the total power generated. In the prototype developed in this work, which for reasons of compactness and visual impact contains a maximum of 4 levels (8 TEMs), it is important to determine whether these 8 thermoelectric modules are before or after the optimum number of modules, so test started with 8 TEMs and were gradually reduced to 6 and 4, as Fig. 8 depicts. In each level, there were 2 modules connected in series with a load electrical resistance of 3.4 Ω per module. Different heat fluxes were supplied to the rope heaters to obtain the desired temperatures in the lower part of the TPCT, with negligible thermal losses thanks to the insulation.

The results of these tests can be seen in Fig. 9, where the total power generated and the average power generated per module for the three heat source temperatures (T_S) are shown for the 4, 3 and 2 level tests.

It can be seen that for the three hot source temperatures studied, the power generated per module decreases as the number of modules increases since as more modules are installed, the total thermal resistance on the cold side decreases, while the thermal resistance on the hot side remains constant. According to the thermal–electrical analogy in Fig. 10, where the thermal resistances of the thermoelectric

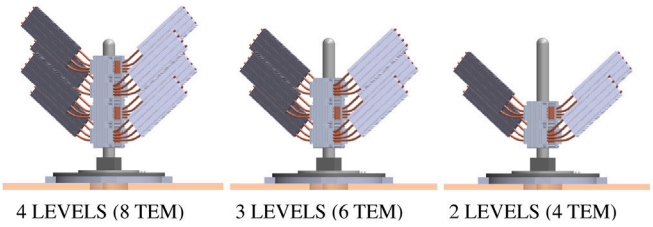

Fig. 8. Schematics of the tests carried out with 8, 6 and 4 TEMs.

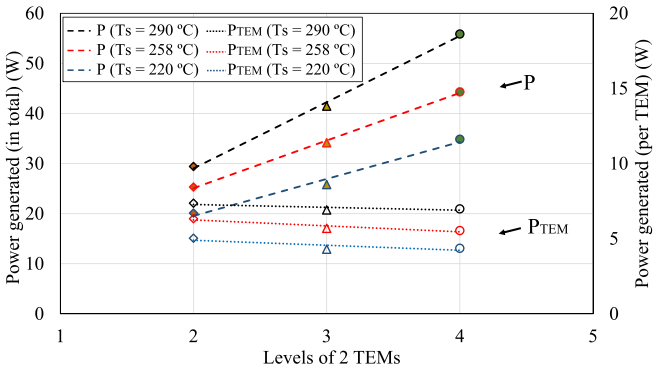

Fig. 9. Results of the generation tests at T_S = 220 °C, T_S = 258 °C *y* T_S = 290 °C with 2, 3 and 4 levels of 2 TEMs in each one.

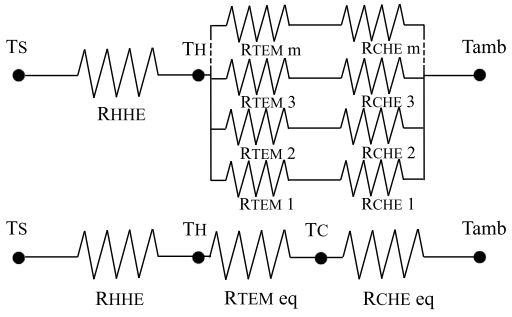

Fig. 10. Electrical analogy of the thermal resistances of the GTEG.

generator have been simplified to the maximum, there is a resistance on the hot side (R_{HHE}), shared by all the thermoelectric modules, one corresponding to each module (R_{TEM}) and another corresponding to the cold side exchanger (R_{CHE}), which each thermoelectric module has one associated. As can be deduced from Eq. (18), an increase in the number of modules means decreasing the term $R_{TEMeq} + R_{CHEeq}$ because they correspond to parallel resistances. The heat flux that the generator is capable of extracting corresponds to Eq. (19), where T_S is the temperature of the heat source and T_{amb} the one of the environment, therefore, if we increase the number of modules (m), $R_{TEMeq} + R_{CHEeq}$ will decrease and so will do the denominator of the equation, therefore $\dot{Q}_H$ will increase. As the heat flow through the generator increases, keeping R_{HHE} constant, the temperature of the hot face of the modules (T_H) decreases according to Eq. (20). This makes the efficiency decrease and, therefore, the power generated by each module (P_{TEM}) also decreases, according to Eq. (21).

$$R_{TEMeq} + R_{CHEeq} = \frac{R_{TEM} + R_{CHE}}{m} \tag{18}$$

$$\dot{Q_H} = \frac{T_S - T_{amb}}{R_{HHE} + R_{TEMeq} + R_{CHEeq}} \tag{19}$$

$$\dot{Q_H} = \frac{T_S - T_H}{R_{HHE}} \tag{20}$$

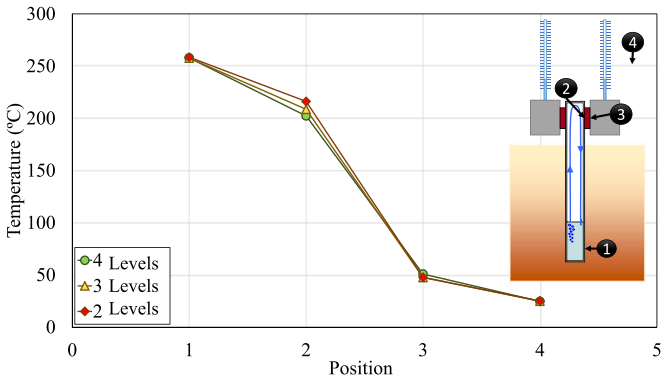

Fig. 11. Temperature drop from the wall of the TPCT (1), the hot side of the TEM (2), the cold side of the TEM (3) and the ambient (4).

$$P_{TEM} = \frac{\dot{Q}_H}{m} - \dot{Q}_C \tag{21}$$

$$P = \dot{Q}_H - \dot{Q}_C \cdot m \tag{22}$$

Although the power generated per module decreases with the increase in the number of modules, the total output power of the generator (P), which corresponds to Eq. (22), increases with the number of modules for the tested values. Moreover, it increases very significantly, up to 90% with 4 module levels compared to 2, in the highest temperature test. In the range of modules studied, the addition of one more level compensates for the decrease in power per module. This means that with 4 levels installed, i.e. with 8 thermoelectric modules, the optimum point of modules from which the total power starts to decrease has not been reached yet. This result is very favourable, as the available space of the thermosyphon protruding from the ground is being used to the maximum, maximizing the compactness of the device.

The temperatures obtained in the T_S = 258 °C test have been represented in Fig. 11 at four points of interest: the temperature of the heat source (*Point*1), the temperature of the hot face of the thermoelectric modules (*Point*2), the temperature of the cold face of the thermoelectric modules (*Point*3) and the ambient temperature (*Point*4). It is observed that, for equal temperature of the hot and cold sources, the temperature of the hot face is higher in the case of 2 levels (T_H = 216.19 °C), followed by that of 3 (T_H = 208.64 °C) and finally that of 4 levels (T_H = 202.33 °C). This corresponds to the explanation given about Fig. 10, since as $R_{TEM}+R_{CHE}$ increases in the 2-level test, for invariant T_S, T_{amb} and R_C, the temperature of the hot face of the modules T_H increases. Meanwhile, the temperature of the cold side (T_C) increases as the number of levels or modules increases, but less than the increase of T_H, since the resistance of the cold side becomes less predominant than the one of the HHE. That is why the different T_C in each test is barely appreciated in Fig. 11. Thus, the fewer modules are installed, the greater the thermal difference between the TEMs faces (Catalan, 2020).

The total power output of the developed thermoelectric generator was plotted as function of the temperature difference between the hot and cold sources. This result is shown in Fig. 12, where it has been represented with the 4, 3 and 2 levels of thermoelectric modules. The highest power value achieved was 55.95 W in total, which is 6.99 W per TEM, with 4 levels (8 modules) and a temperature difference between the thermosyphon wall and the environment of 269 °C. For the same temperature difference, the power obtained with 3 levels (6 modules) was 42.21 W (7 W per TEM), and with 2 levels (4 modules) 29.10 W (7.27 W per TEM). Fig. 13, it can be seen that the maximum efficiency in the transformation of a heat flow into electricity ($\eta = fracP\dot{Q}$) is achieved when two levels of modules are installed, with a value greater than 5%. In the case of 3 and 4 module levels, the maximum efficiency

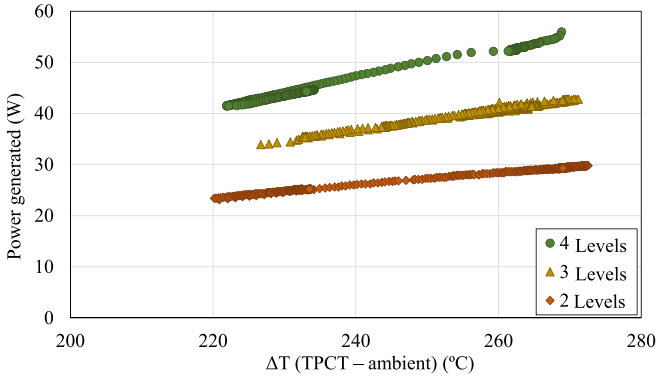

Fig. 12. Total generated power depending on the temperature difference between the wall of the TPCT and the ambient.

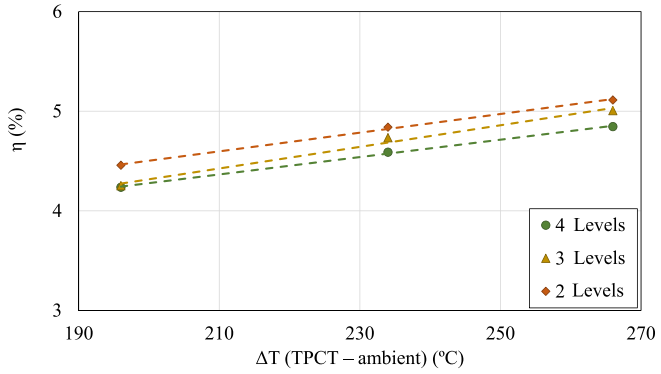

Fig. 13. Efficiency of the GTEG depending on the temperature difference between the wall of the TPCT and the ambient.

per module decreases to 5 and 4.8% respectively. If we take into account the intermediate temperature tested (temperature difference between sources of 235 °C), the efficiency values obtained are between 4.59% and 4.83%, which are very high efficiency values compared to the GTEGs existing in the literature.

4. Field installation and results

Thanks to the tests carried out in the laboratory, the correct operation of the thermoelectric generator for high-temperature geothermal energy was ensured. After determining that the highest generated power was achieved with 4 levels (8 thermoelectric modules), compared to the obtained with 3 and 2 levels, the generator was reassembled and shipped to the Timanfaya National Park, where its installation were carried out.

4.1. Installation and commissioning

Fig. 14 shows the generator finally installed, with the four levels of thermoelectric modules, i.e. 8 TEMs in total, each with its corresponding heat exchanger on the cold side.

The device was installed in the S-5 borehole in Fig. 15, whose temperature profile is shown in Fig. 1. Firstly, the base and the fastenings were placed and the temperature of the hot gases was measured, which reached 464 °C, as Fig. 16 shows.

In the installation, the generator was oriented towards the predominant wind direction (N-NE) to take maximum advantage of convection and the GTEG was anchored to the base the deflector, which directs the hot exit gases at a distance of 0.5 m from the generator. The base was insulated so that heat would not reach the heat exchangers

Fig. 14. Geothermal thermoelectric generator for high temperature geothermal anomalies installed in *Islote Hilario* (Timanfaya National Park, Lanzarote).

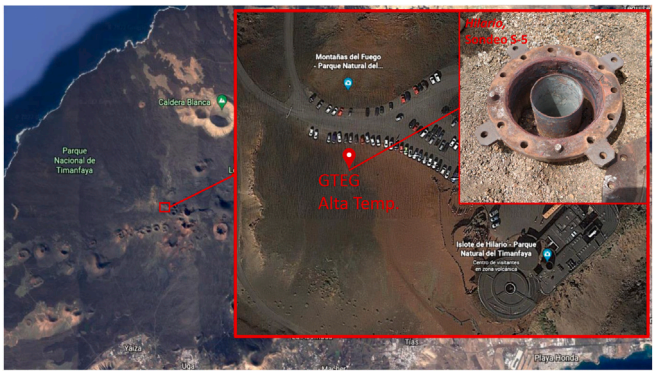

Fig. 15. Location of the HT-GTEG in *Islote Hilario* (Timanfaya National Park).

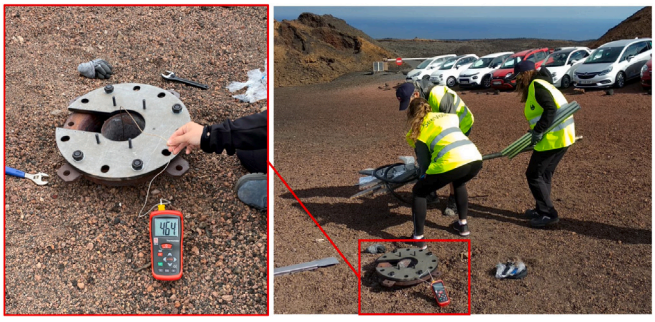

Fig. 16. Borehole and temperature measurement.

on the cold side of the lower levels. The positions of the instruments for measuring the temperature, voltage and current of the modules and the wind speed/direction were are shown in Fig. 17. One sensor measures the air temperature inside the borehole (T_{air}), two measure the temperature of the thermosyphon inside the borehole (T_{t1} and T_{t2}) and two other measure the module face temperatures (T_H and T_C) at each level. In addition, the voltage (V) and current (I) generated by the two modules connected in series are also measured at each level. Finally, one more sensor measures the ambient temperature and an anemometer measures the wind speed. After the entire device reached a temperature above 100 °C, the thermosyphon was purged to remove any air that might remain inside and that would impair the operation of the device.

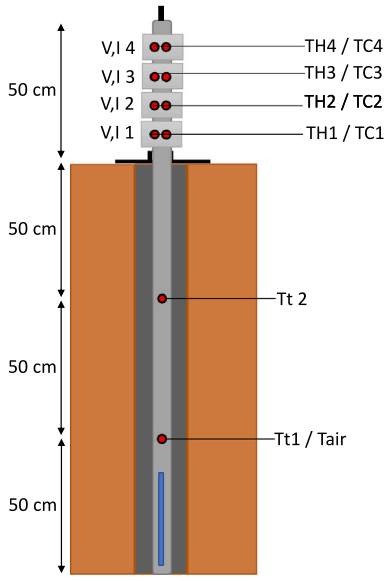

Fig. 17. Distribution of the sensors in the HT-GTEG installed in field.

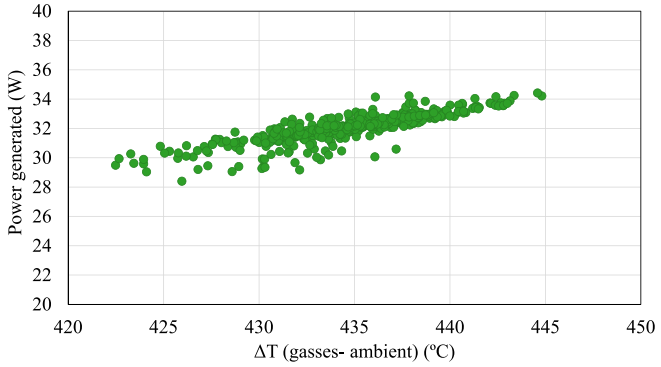

Fig. 18. Generated power in field versus the temperature difference between the heat source and the ambient.

4.2. Operation and results

After successfully installing and commissioning the generator in the TNP, it has been working correctly, continuously and without the need for maintenance since June 2021 (for more than one year), which is a very important achievement for a geothermal thermoelectric generator installed in field, as there are not other GTEGs in the literature installed in a geothermal field with such high temperatures. It is a very robust device due to the absence of moving parts. The maximum power generation was obtained in November 2021 with 36 W in total (4.5 W/TEM), with a temperature difference between the gases and the ambient of 444 °C and a wind velocity of 10 km/h.

Fig. 18 shows the average values (every 2 h during the first 3 working months) of the total generated power with respect to the temperature difference between the heat source (air leaving the borehole) and the cold source (the environment). This figure clearly shows the linear increasing tendency of the output power with the temperature difference, which is exactly the same tendency as in the laboratory (see Fig. 12), although the hot source in this case is a mixture of gases. Despite the linear tendency, there exists a deviation caused by changes in the wind velocity and, thus, in the CHEs thermal resistance.

In order to observe how the power generated depends on the ambient temperature and on the wind, the average value of the power generated every two hours, the wind speed and the ambient temperature during a month of operation are represented in Fig. 19. Here,

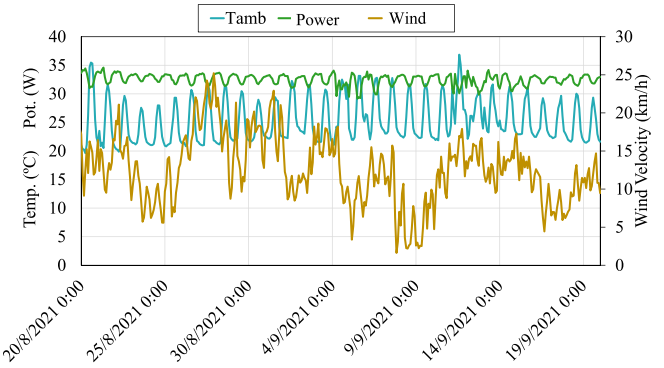

Fig. 19. Power generated by the GTEG, ambient temperature and wind speed during one month in 2021.

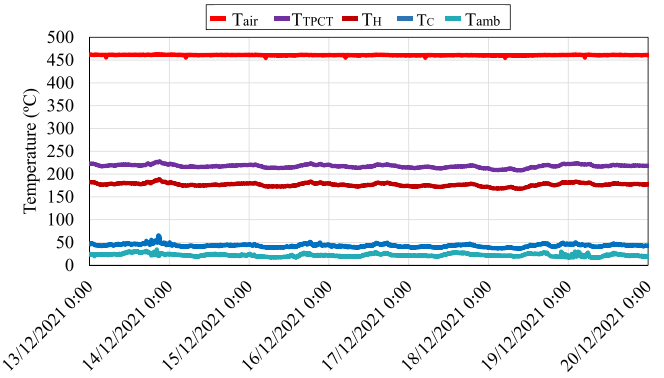

Fig. 20. Registered temperatures in the GTEG.

the power generated varies with the ambient temperature, presenting generation peaks at night, when the ambient temperature is lower, and the power valleys occur during the central hours of the day because the ambient temperature is higher.

Fig. 20 shows the temperatures measured at various points on the generator during one week of operation. These points are the air temperature coming from the borehole (T_{air}), the ambient temperature (T_{amb}), the temperatures of the hot (T_h) and cold (T_c) side of the thermoelectric modules, and also the outside temperature of the lower wall of the thermosyphon (T_t). It can be seen that the temperature of the geothermal heat source is constant and equal to 460 °C. From an available temperature difference between sources of approximately 435 °C constant, the difference achieved between the TEMs' faces is 155 °C. On the cold part, the temperature differs by less than 20 °C between the cold face of the module and the ambient, which is totally successful considering that this CHE is completely passive. On the TEM's hot side, however, there is a very significant temperature drop of 285 °C from the heat source. That is normal and the main reason is the high convection resistance with the air inside the borehole, as temperature T_t shows, which experiences a drop of 246 °C with respect to the temperature of the gases. The equation corresponding to the convective heat transfer between the borehole gases and the thermosyphon is Newton's Cooling Law, which, applied to this system, is Eq. (23). Given that the air leaves the borehole at a constant temperature T_{air} of 460 °C and with a constant convection coefficient h, to achieve a higher temperature in the thermosyphon T_t, the convective heat transfer area A_{conv} should be increased, so it would be convenient to include fins in the boiling zone of the TPCT to increase the convective area between the thermosyphon and the air leaving the borehole.

$$\dot{Q} = h \cdot A_{conv} \cdot (T_{air} - T_t) \tag{23}$$

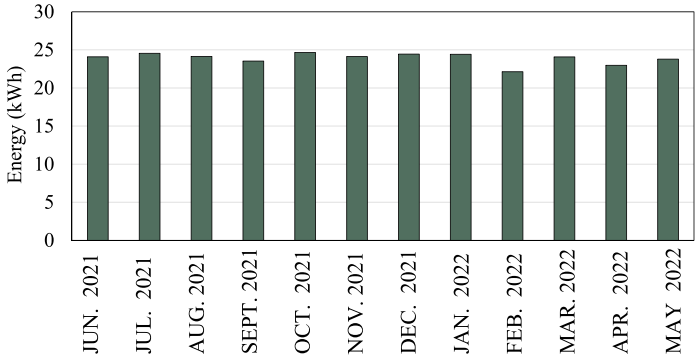

Fig. 21. Generated electrical energy during one year.

Table 4
Average values of efficiency and thermal resistances of the GTEG.

P (W)	34.14
P/TEM (W)	4.27
$\Delta T_{(H-C)}$ (°C)	133.05
η (%)	4.28
$\dot{Q}_H$ (W)	797.20
$R_{HHE_{conv}}$ (K/W)	0.252
$R_{HHE_{int}}$ (K/W)	0.11
R_{CHE} (K/W)	0.215

The average efficiency of the GTEG developed was calculated following Eq. (24), as well as the thermal resistances of the hot and cold side heat exchangers. The results are shown in Table 4 for a day in January 2022 when the average ambient temperature was 18 °C and the average wind speed was 20.5 km/h, similar values to the average annual conditions in Lanzarote (21 °C and 21.6 km/h). The efficiency obtained in this thermoelectric generator is 4.28%, managing to convert into electrical energy a heat flow transported by very efficient heat exchangers with resistances of 0.11 K/W as the internal thermal resistance of the hot side and 0.215 K/W per module the cold side (0.027 K/W the total equivalent thermal resistance of the cold side). This efficiency is very close to the maximum given by the datasheet, which is 4.97%, so it is a very good result, even though the highest thermal resistance is the one of convection with the gases ($R_{HHE_{conv}} = 0.252$ K/W) due to the low density and convection coefficient of the gases. If this resistance was lowered by including fins, the efficiency would be even better. Although the efficiency is far from the one that conventional geothermal plants can achieve (~20%) (Breede et al., 2013), the reached value here is great for a thermoelectric generator, taking into account that this device presents important advantages such as the low environmental impact and the possibility for self-consumption.

$$\eta = \frac{P}{\dot{Q}_H} \tag{24}$$

Finally, to determine the feasibility of this technology on a large scale, it is very important to determine how much energy the developed GTEG can generate each year. Therefore, the energy generated every month was calculated for a complete year from June 2021 until May 2022, which is plotted in Fig. 21. As seen, the monthly produced energy is steady, with few fluctuations over the months, where the maximum difference in power generated is 10% between the month that generated the most power (October) and the month that generated the least (February). The total energy generated by this high-temperature GTEG is of 286.94 kW h per year. Given that the area occupied is 0.75 m^2, the annual electrical energy per unit of area is 382.59 kW h/m^2, 5 times higher than a PV panel occupating the same area (European Comission, 2022), given the continuity of geothermal energy.

5. Conclusions

The developed GTEG was successfully installed in a borehole in the area with the most extreme registered temperatures in the Timanfaya National Park, with gases reaching 465 °C, and where this device has been operating continuously and without the need for maintenance for more than one year.

First of all, a computational model was employed to design the hot side heat exchanger, which consists in a two phase closed thermosyphon with water as the working fluid. After characterizing the cold side heat exchanger, that also works by phase change, the generator was tested in the laboratory. Tests were carried out with different temperatures in the wall of the TPCT, reaching 290 °C, and varying the number of thermoelectric modules installed. It was determined that, as the number of thermoelectric modules installed in the thermosyphon increases, the power generated by each one decreases. However, for the values of modules studied here, this effect is compensated by adding more modules, so the total power increases. Thus, the thermosyphon with 8 modules distributed in pairs along 4 levels was the configuration that allowed the maximum power generated in the laboratory.

Given the good laboratory results, the thermoelectric generator with 8 modules was successfully installed in the area of highest surface temperatures of the Timanfaya National Park. After more than 12 months in perfect field operation, the maximum power generation was 36 W (4.5 W/TEM), with a temperature difference between the gases and the ambient of 444 °C and a wind velocity of 10 km/h. The installed cold side heat exchangers are very efficient, with a thermal resistance of 0.215 K/W per module. The heat exchanger on the hot side has a internal thermal resistance of 0.11 K/W, which is very successful. Thus, phase change heat exchangers are completely adequate for this application, as they transport heat very efficiently and they do not require moving parts nor auxiliary consumption. In any case, the high difference between the gases and the TPCT (of 246 °C) is caused by the convective thermal resistance of 0.252 K/W, because there is a heat transmission by convection with gases, which have low values of convective coefficient. This convective thermal resistance could only be improved by increasing the convective area of the boiling part of the thermosyphon.

The efficiency of this GTEG in field is 4.28%, close to the maximum value given by the TEMs manufacturer, managing to generate an energy of more than 286.94 kW h per year (382.59 kW h/m^2), thus demonstrating not only the viability of this technology, but also the great potential that exists for transforming the geothermal energy of the island of Lanzarote into renewable electricity. Furthermore, this robust generator does not require maintenance nor auxiliary consumption, which reduces its costs, and produces a minimal environmental impact, it is noiseless, and the use of water as working fluid makes it completely harmless.

To conclude, this development demonstrates that it is viable to use this technology to generate clean energy in an area with high temperature geothermal anomalies, with very favourable results in terms of energy generation.

CRediT authorship contribution statement

Patricia Alegría: Investigation, Data curation, Formal analysis, Writing – original draft, Writing – review & editing. **Leyre Catalán:** Methodology, Software, Writing – review & editing. **Miguel Araiz:** Conceptualization, Methodology, Investigation. **Álvaro Casi:** Software, Validation. **David Astrain:** Conceptualization, Funding acquisition, Project administration, Supervision.

Declaration of competing interest

The authors declare that they have no known competing financial interests or personal relationships that could have appeared to influence the work reported in this paper.

Data availability

Data will be made available on request.

Acknowledgements

We would like to acknowledge the support of the Spanish State Research Agency and FEDER-UE funds under the grants TED2021-129359B-I00 and PID2021-124014OB-I00. Open access funding provided by Universidad Pública de Navarra.

References

Ahiska, R., Mamur, H., 2013. Design and implementation of a new portable thermoelectric generator for low geothermal temperatures. IET Renew. Power Gener. 7, 700–706. http://dx.doi.org/10.1049/iet-rpg.2012.0320.

Alegria, P., Catalan, L., Araiz, M., Rodriguez, A., Astrain, D., 2022. Experimental development of a novel thermoelectric generator without moving parts to harness shallow hot dry rock fields. Appl. Therm. Eng. 200, http://dx.doi.org/10.1016/j.applthermaleng.2021.117619.

Arana, V., Ortiz, R., Yuguero, J., 1973. Thermal anomalies in Lanzarote (Canary Islands).

Breede, K., Dzebisashvili, K., Liu, X., Falcone, G., 2013. A systematic review of enhanced (or engineered) geothermal systems: past, present and future. Geotherm. Energy 1, http://dx.doi.org/10.1186/2195-9706-1-4.

Casi, A., Araiz, M., Catalan, L., Astrain, D., 2020. Thermoelectric heat recovery in a real industry: From laboratory optimization to reality. Appl. Therm. Eng. http://dx.doi.org/10.1016/j.applthermaleng.2020.116275.

Catalan, L., 2020. Design and experimental development of thermoelectric generators for shallow geothermal anomalies of volcanic origin.

Catalan, L., Araiz, M., Aranguren, P., Astrain, D., 2020a. Computational study of geothermal thermoelectric generators with phase change heat exchangers. Energy Convers. Manage. 221, http://dx.doi.org/10.1016/j.enconman.2020.113120.

Catalan, L., Araiz, M., Aranguren, P., Padilla, G.D., Hernandez, P.A., Perez, N.M., de la Noceda, C.G., Albert, J.F., Astrain, D., 2020b. Prospects of autonomous volcanic monitoring stations: Experimental investigation on thermoelectric generation from fumaroles. Sensors (Switzerland) 20, 1–21. http://dx.doi.org/10.3390/s20123547.

Catalan, L., Aranguren, P., Araiz, M., Perez, G., Astrain, D., 2019. New opportunities for electricity generation in shallow hot dry rock fields: A study of thermoelectric generators with different heat exchangers. Energy Convers. Manage. 200, http://dx.doi.org/10.1016/j.enconman.2019.112061.

Catalan, L., Garacochea, A., Casi, A., Araiz, M., Aranguren, P., Astrain, D., 2020c. Experimental evidence of the viability of thermoelectric generators to power volcanic monitoring stations. Sensors (Switzerland) 20, 1–25. http://dx.doi.org/10.3390/s20174839.

Champier, D., 2017. Thermoelectric generators: A review of applications. Energy Convers. Manage. 140, 167–181. http://dx.doi.org/10.1016/j.enconman.2017.02.070.

Coleman, H., Steele, W., 2018. Experimentation, Validation and Uncertainty. Analysis for Engineers, third ed..

Dell, R., Wei, C.S., Petralia, M.T., Gislason, G., Unnthorsson, R., 2018. Thermoelectric powered security systems in Iceland using a geothermal steam pipe as a heat source. Proceedings 2, 440. http://dx.doi.org/10.3390/icem18-05309.

European Comission, 2020. European Green Deal. 2050 long-term strategy. URL https://ec.europa.eu/clima/eu-action/climate-strategies-targets/2050-long-term-strategy_en.

European Comission, 2022. Photovoltaic geographical information system. URL https://re.jrc.ec.europa.eu/pvg_tools/en/.

Forster, H., Zuber, N., 1955. Dynamics of vapour bubbles and boiling heat transfer. Am. Inst. Chem. Eng. J. 1, 531–535.

Ganguly, S., Kumar, M.S.M., 2012. Geothermal reservoirs-A brief review.

Garcia, A., Romero, C., Ortiz, R., Doniz, J., Carmona, J., Martinez-Arevalo, C., Garcia-Cacho, L., 2009. Investigación volcanológica en el parque nacional de timanfaya (lanzarote, islas canarias). Generación y tratamiento de bases de datos geofísicos y geomorfológicos para su integración en los programas de gestión. In: Proyectos de Investigación En Parques Nacionales: 2005-2008. Ministerio de Medio Ambiente, Medio Rural y Marino, Organismo Autónomo de Parques Nacionales, URL https://www.miteco.gob.es/images/es/oapn_inv_art_0501_tcm30-65677.pdf.

Government of the Canary Islands, 2019. Plan de transición energética de Canarias. URL https://www.canariastransicionecologica.com/transicion-energetica/normas-y-planes-transicion-energetica/plan-de-transicion-energetica-de-canarias/.

Government of the Canary Islands, 2021. Geothermal strategy in the Canary Islands.

Government of the Canary Islands, MITECO, IDAE, 2022. Sustainable energy strategy in the Canary Islands.

Instituto Geológico Minero Español, 1992. Evaluación del Potencial Geotérmico Superficial de Montañas de Fuego como Sistema de Roca Caliente Seca. Tech. rep..

Lemmon, E., Bell, I., Huber, M., McLinden, M., 2018. NIST standard reference database 23: Reference fluid thermodynamic and transport properties-REFPROP, version 10.0. http://dx.doi.org/10.18434/T4JS3C, URL https://www.nist.gov/srd/refprop.

Li, K., Bian, H., Liu, C., Zhang, D., Yang, Y., 2015. Comparison of geothermal with solar and wind power generation systems. Renew. Sustain. Energy Rev. 42, 1464–1474. http://dx.doi.org/10.1016/j.rser.2014.10.049.

Li, K., Garrison, G., Zhu, Y., Moore, M., Liu, C., Hepper, J., Bandt, L., Horne, R., Petty, S., 2021. Thermoelectric power generator: Field test at Bottle Rock geothermal power plant. J. Power Sources 485, http://dx.doi.org/10.1016/j.jpowsour.2020.229266.

Ministerio para la Transición Ecológica y el Reto Demográfico, 2020. Plan nacional integrado de energía y clima. URL https://www.miteco.gob.es/es/prensa/pniec.aspx.

Mona, Y., Do, T.A., Sekine, C., Suttakul, P., Chaichana, C., 2022. Geothermal electricity generator using thermoelectric module for IoT monitoring. Energy Reports 8, 347–352. http://dx.doi.org/10.1016/j.egyr.2022.02.114.

Red Eléctrica de España, 2021. El sistema eléctrico español: Avance 2021. URL https://www.ree.es/es/glosario.

REN21, 2021. Renewables 2020. Global Status Report, REN21 Secretariat.

Rohsenow, W., Hartnett, J., Cho, Y., 1998. Handbook of Heat Transfer, third ed. McGraw-Hill Handbooks.

Saberi, Y., Sajjadi, S.A., 2022. A comprehensive review on the effects of doping process on the thermoelectric properties of Bi2Te3 based alloys. J. Alloys Compd. 904, http://dx.doi.org/10.1016/j.jallcom.2022.163918.

Sandvik, 2022. Hydraulic and instrumentation tubing for the petrochemicals and oil and gas industries. URL https://www.materials.sandvik/es-es/productos/tube-pipe-fittings-and-flanges/tubular-products/instrumentation-tubing/.

Suter, C., Jovanovic, Z.R., Steinfeld, A., 2012. A 1kWe thermoelectric stack for geothermal power generation - Modeling and geometrical optimization. Appl. Energy 99, 379–385. http://dx.doi.org/10.1016/j.apenergy.2012.05.033.

Troll, V.R., Carracedo, J.C., 2016. The geology of Lanzarote. http://dx.doi.org/10.1016/b978-0-12-809663-5.00007-4.

United Nations, 2016. Paris Agreement signed by parties to the United Nations Framework Convention on Climate Change.

Zhao, Y., Fan, Y., Li, W., Li, Y., Ge, M., Xie, L., 2022. Experimental investigation of heat pipe thermoelectric generator. Energy Convers. Manage. 252, 115123. http://dx.doi.org/10.1016/j.enconman.2021.115123.